The University of Southern Mississippi

The Aquila Digital Community

10-1-2012

Modeling Photosynthesis of *Spartina alterniflora* (Smooth Cordgrass) Impacted by the Deepwater Horizon Oil Spill Using Bayesian Inference

Wei Wu
University of Southern Mississippi, Wei.Wu@usm.edu

Patrick D. Biber
University of Southern Mississippi, patrick.biber@usm.edu

Mark S. Peterson
University of Southern Mississippi, mark.peterson@usm.edu

Chongfeng Gong
University of Southern Mississippi, Chongfeng.Gong@usm.edu

Follow this and additional works at: https://aquila.usm.edu/fac_pubs

Part of the Marine Biology Commons

Modeling photosynthesis of *Spartina alterniflora* (smooth cordgrass) impacted by the Deepwater Horizon oil spill using Bayesian inference

You may also be interested in:

The weathering of oil after the Deepwater Horizon oil spill: insights from the chemical composition of the oil from the sea surface, salt marshes and sediments
Zhanfei Liu, Jiqing Liu, Qingzhi Zhu et al.

Effects of oil on the rate and trajectory of Louisiana marsh shoreline erosion
Giovanna McClenachan, R Eugene Turner and Andrew W Tweel

Tidal influences on carbon assimilation by a salt marsh
James C Kathilankal, Thomas J Mozdzer, Jose D Fuentes et al.

Evolution of the optical properties of seawater influenced by the Deepwater Horizon oil spill in the Gulf of Mexico
Zhengzhen Zhou and Laodong Guo

Linking ramped pyrolysis isotope data to oil content through PAH analysis
Matthew A Pendergraft, Zeynep Dincer, José L Sericano et al.

Global change accelerates carbon assimilation by a wetland ecosystem engineer
Joshua S Caplan, Rachel N Hager, J Patrick Megonigal et al.

Modeling photosynthesis of *Spartina alterniflora* (smooth cordgrass) impacted by the Deepwater Horizon oil spill using Bayesian inference

Wei Wu, Patrick D Biber, Mark S Peterson and Chongfeng Gong

Department of Coastal Sciences, The University of Southern Mississippi, 703 East Beach Drive, Ocean Springs, MS 39564, USA

E-mail: wei.wu@usm.edu

Abstract

To study the impact of the Deepwater Horizon oil spill on photosynthesis of coastal salt marsh plants in Mississippi, we developed a hierarchical Bayesian (HB) model based on field measurements collected from July 2010 to November 2011. We sampled three locations in Davis Bayou, Mississippi (30.375°N, 88.790°W) representative of a range of oil spill impacts. Measured photosynthesis was negative (respiration only) at the heavily oiled location in July 2010 only, and rates started to increase by August 2010. Photosynthesis at the medium oiling location was lower than at the control location in July 2010 and it continued to decrease in September 2010. During winter 2010–2011, the contrast between the control and the two impacted locations was not as obvious as in the growing season of 2010. Photosynthesis increased through spring 2011 at the three locations and decreased starting with October at the control location and a month earlier (September) at the impacted locations.

Using the field data, we developed an HB model. The model simulations agreed well with the measured photosynthesis, capturing most of the variability of the measured data. On the basis of the posteriors of the parameters, we found that air temperature and photosynthetic active radiation positively influenced photosynthesis whereas the leaf stress level negatively affected photosynthesis. The photosynthesis rates at the heavily impacted location had recovered to the status of the control location about 140 days after the initial impact, while the impact at the medium impact location was never severe enough to make photosynthesis significantly lower than that at the control location over the study period. The uncertainty in modeling photosynthesis rates mainly came from the individual and micro-site scales, and to a lesser extent from the leaf scale.

Keywords: Deepwater Horizon oil spill, photosynthesis, salt marsh, hierarchical Bayesian models, multi-scale

S Online supplementary data available from stacks.iop.org/ERL/7/045302/mmedia

1. Introduction

Coastal wetlands are among the most productive ecosystems in the world, providing benefits such as carbon sequestration,

storm protection, flood control, habitat, improved water quality, and recreational and aesthetic opportunities (Engle 2011, Jordan and Peterson 2012). However, coastal wetlands and their ecosystem services are not only threatened by upland stressors (Peterson and Lowe 2009), but they are also at risk from ocean-side stressors, in particular accelerated sea-level rise, erosion and anthropogenic pollutants like occasional oil spills.

The Deepwater Horizon (DWH) oil spill in the northern Gulf of Mexico (GOM), from 20 April to 15 July 2010, was the largest marine oil spill in the history of the petroleum industry (available at http://en.wikipedia.org, accessed on 16 March 2012). This accident released about $4.4 \times 10^6 \pm 20\%$ barrels (7.0×10^6 m^3) of crude oil into the ocean from the well at 1500 m depth (Crone and Tolstoy 2010). Crude oil degrades in water via evaporation, dissolution, emulsification, sedimentation, biodegradation (microbial oxidation) and photooxidation (e.g., Hunt 1996, Fingas 1999, Plata *et al* 2008, Mendelssohn *et al* 2012, Liu *et al* 2012) before coming ashore. On the Mississippi Gulf Coast, small oil slicks (<100 m^2) arrived sporadically from early June 2010 through 2011 but slicks arrived onshore more frequently and as larger patches during active tropical systems (e.g., Hurricane Alex, TS Bonnie and TD #5; http://www.nhc.noaa.gov/2010atlan.shtml, accessed on 16 March 2012).

The response of vegetation in coastal wetlands to weathered crude oil is complex and variable, ranging from short-term reductions in photosynthesis and rapid subsequent recovery, to complete mortality and long-term wetland loss (Pezeshki *et al* 2000, 2001, Roth and Baltz 2009, Engle 2011). Oil can affect plants directly by coating the leaves and blocking stomata, it's chemical toxicity disrupts plant–water relations or directly impacts the living cells, and it reduces oxygen exchange between the atmosphere and the soil with negative consequences for root health (Baker 1970, Pezeshki *et al* 2000, Ko and Day 2004). Spilled oil can also increase temperature stress, which combined with reduced photosynthetic gas exchange, will cause acute impacts (Baker 1970, Lin and Mendelssohn 1996, Ko and Day 2004). The acute impacts vary depending on the amount and type of oil, oiling frequency, the weather and hydrologic conditions, the species of plant, the spatial extent of oil coverage, season, soil composition and cleanup activity (Lin and Mendelssohn 1996, Hester and Mendelssohn 2000, Pezeshki *et al* 2000, Mendelssohn *et al* 2012). *Spartina alterniflora* (smooth cordgrass) was more sensitive to partial oil coating than *Juncus roemerianus* (black needlerush; Pezeshki and DeLaune 1993), both plant species are important on the US Gulf Coast. In contrast, moderate oiling from the DWH oil spill had no significant effect on *Spartina* although it significantly lowered live above-ground biomass and stem density of *Juncus* in the Bay Jimmy, northern Barataria Bay, Louisiana (Lin and Mendelssohn 2012). Furthermore, *S. alterniflora* and *Sagittaria lancifolia* (bulltongue arrowhead) were shown to be more sensitive to oiling during the spring/summer growing season than during the pre-dormancy or dormant season in winter (Pezeshki *et al* 2000, Mishra *et al* 2012). This notwithstanding, salt marshes in the northern

GOM region can recover rapidly (Pezeshki and DeLaune 1993, Pezeshki *et al* 2000).

However, oil spills can cause adverse chronic consequences on coastal wetlands and adjacent aquatic habitats due to oil penetration into the sediment and persistence in it (Krebs and Tanner 1981, Alexander and Webb 1987, Lin and Mendelssohn 1998, Mendelssohn *et al* 2012). The severity of chronic impacts is influenced by the volume and chemical nature of the oil, the oil's amount of contact with and penetration of the soil, the physical nature of the coastline (high or low energy) and the composition of the plant community (Dicks and Hartley 1982, Ko and Day 2004, Mendelssohn *et al* 2012). Once oil penetrates the sediment, the recovery to reference conditions may take 3–4 years (Alexander and Webb 1987, Mendelssohn *et al* 1993, Hester and Mendelssohn 2000) or longer (Bergen *et al* 2000, Michel *et al* 2009, Mendelssohn *et al* 2012). Under extreme circumstances, recovery may never occur due to sediment removal (Baca *et al* 1987, Gilfillan *et al* 1995) or accelerated erosion after vegetation morality (Mendelssohn *et al* 2012). Even after plants resume growth, oil may continue to adversely affect soil microbial functions in coastal wetlands (Burns and Teal 1979, Pezeshki *et al* 2001). Understanding the acute and chronic impacts of oil on coastal wetlands is important to be able to assess their resilience.

Net primary productivity is an aggregate measure of energy available to support ecosystem structure and function (Cardoch *et al* 2002); therefore, photosynthesis can be used to assess the impact of oil on ecosystem health. However, inferring how photosynthesis is affected by chronic and indirect exposure to oil can be difficult because of spatial and temporal complexity. On the one hand, factors at multiple spatial scales (from cm to km) will influence photosynthesis, from individual-plant level traits (cm), to site-specific variation (m), to the broader landscape level (km). On the other hand, photosynthesis changes over time as a response to seasonal patterns, with more photosynthesis during the growing season and less in the dormant season. The difficulty inherent in relating the change in photosynthesis rates directly to a specific oil spill will increase with the scale and complexity of the ecosystem as well as additional disturbance/stress factors such as sea-level rise (Fabricius and De'Ath 2004) unrelated to the oil spill event. A coherent way to link these various processes occurring simultaneously at multiple spatial and temporal scales is therefore necessary to better elucidate the oil-related impacts on photosynthesis during the chronic stress phase of recovery.

Recent advances in computational statistics have produced new tools for inference and prediction, such as the hierarchical Bayesian (HB) modeling approach. This approach has the capacity to exploit diverse sources of information, can accommodate uncertainties, and has the ability to draw inferences on large numbers of latent (inferred) variables and parameters that describe complex relationships (Clark 2005). The approach accommodates complex systems by decomposing their high-dimensional relationships into levels of conditional distribution within a consistent framework: data level, process model level
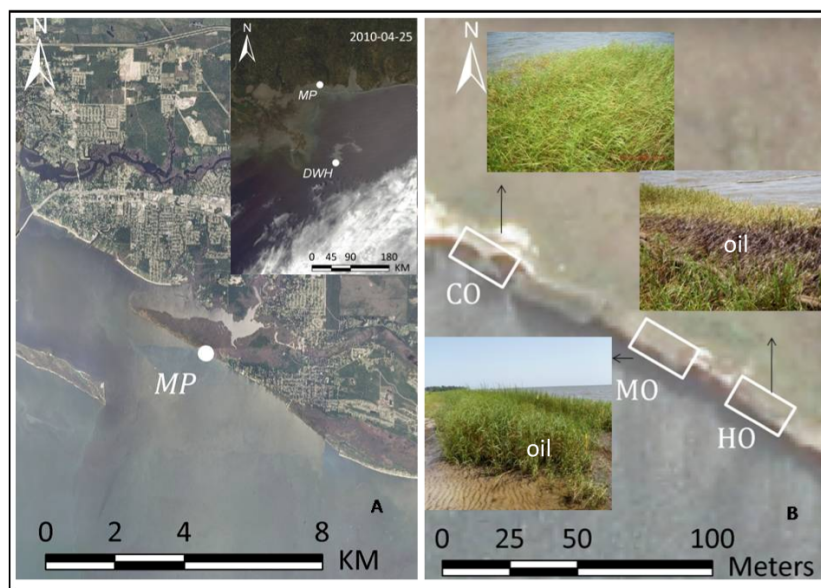
Figure 1. Multiple-scale images of the study area. (A) Marsh Point's (MP) general location at the southern border of Davis Bayou, Ocean Springs, MS (digital orthophoto quadrangle, November 2010, courtesy of MARIS[1]). The inset shows the location of MP relative to the Deepwater Horizon (DWH) and early oil slick (MODIS Aqua image, 25 April 2010). (B) The three locations we sampled at MP: control (CO), medium oiled (MO) and heavily oiled (HO), with photos of the vegetation status on July 2010, 13 days after the first oiling. Note the north arrow on (B) does not apply to orientation of the three vegetation photos.

and parameter level (Clark *et al* 2001). In particular, the process model is made stochastic, consistent with the system complexity, and our limited understanding of the processes (e.g., photosynthesis in our study). The stochasticity allows us to impose conditional independence at the data level and assimilate the relationships among state variables at the process level (Wu *et al* 2010). Finally, the simulation results are rich (e.g., posterior distributions instead of point estimates) and the interpretation is simplified because uncertainty can be readily quantified using credible intervals from the resulting posteriors.

In this study, we aim to

(1) Develop an HB statistical model to simulate photosynthesis of *S. alterniflora* plants at three locations representative of a range of oil spill impacts based on field measurements.

(2) Apply the model to infer when photosynthesis of *S. alterniflora* at the oil impacted locations recovered to the status of the control location with inherent leaf, individual, micro-site and seasonal variability accounted for, and which spatial scale contributed the most to variability in the photosynthesis simulations.

2. Methodology

2.1. Study area

We sampled three locations, about 300 m^2 each, at Marsh Point in Davis Bayou, along the southern edge

of the peninsula that forms the southern border of Davis Bayou, on the Mississippi Gulf Coast (30.375°N, 88.790°W, figure 1(A)). One location was not impacted by crude oil (control location, figure 1(B)), the second location experienced medium impact by crude oil (some oil observed on the sediment and plants, figure 1(B)) and the third location was heavily impacted by oil (plants covered by crude oil extensively, figure 1(B)). The spatial extent of the heavy impact area was not larger than about 10 m × 5 m (50 m^2).

Mississippi Gulf Coast's climate is subtropical maritime (Eleuterius 1998), with mean spring, summer, fall and winter temperatures being 19.4 °C, 27.4 °C, 20.4 °C and 11.1 °C, respectively (Reuscher 1998). The area receives an average of 1488 mm of rainfall per year (Eleuterius 1998) with the Hurricane season being from June through November.

The lower, mesohaline area of Davis Bayou is composed of zones of salt marsh vegetation, including mid-marsh *J. roemerianus* and low-marsh water-fringing *S. alterniflora* zones (http://www.dmr.ms.gov/mississippi-gems/210-davis-bayou, accessed on 19 September 2012). Salt-meadow grass (*Spartina patens*) forms narrow bands adjacent to dunes or uplands, and Olneyi bulrush (*Schoenoplectus americanus*) and salt marsh bulrush (*Schoenoplectus robustus*) can be found interspersed with saltgrass (*Distichlis spicata*).

2.2. Field monitoring

We randomly chose 10–15 individuals of *S. alterniflora* at each of the three locations monthly between July 2010 and November 2011 and measured the photosynthesis rate on the middle portion of the second leaf from the tip of each individual using an LI-6400 XT portable photosynthetic

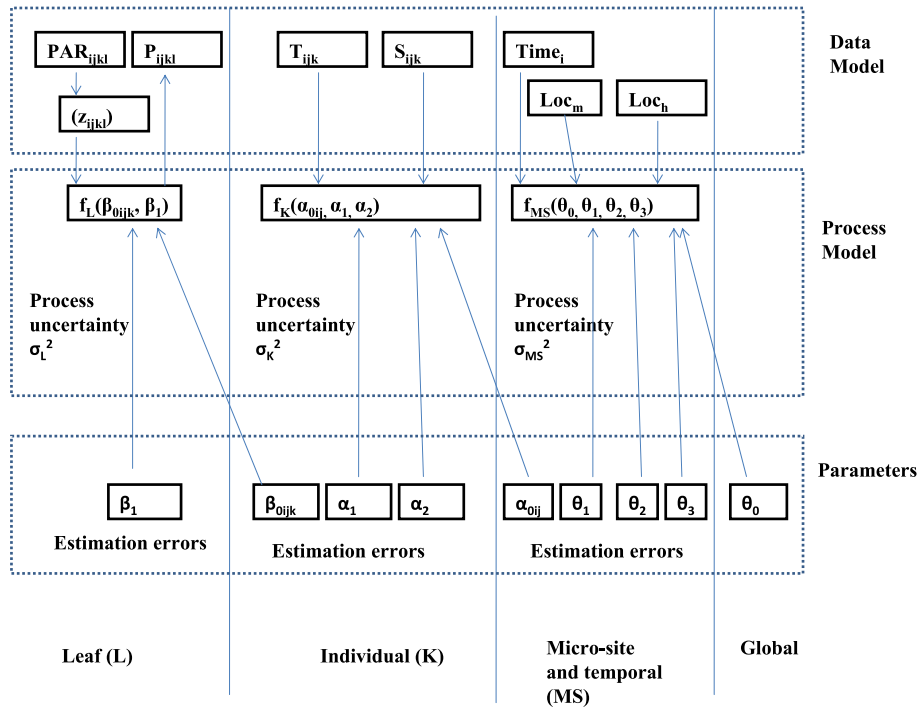[1] Mississippi Automated Resource Information System.

Figure 2. The conceptual model to illustrate the hierarchical structure with complexity decomposed into stages of data, process and parameters (vertical direction) and the association of different spatial scales (horizontal direction). (Adapted from Clark and LaDeau (2006) and McMahon and Diez (2007).)

gas exchange and chlorophyll fluorescence system. The photosynthetic rates for each of the leaves were measured by CO_2 exchange under five identical photosynthetically active radiation (PAR) intensities: ~400 μmol photon m^{-2} s^{-1}, 800 μmol m^{-2} s^{-1}, 1200 μmol m^{-2} s^{-1}, 1600 μmol m^{-2} s^{-1} and 2000 μmol m^{-2} s^{-1} to standardize the photosynthesis rate under saturating light intensities. For each leaf we also measured chlorophyll fluorescence (F_v/F_m) after at least 30 min dark adaption and used this as an indicator of leaf and individual stress or health (Naumann *et al* 2007). Air temperature was recorded by the LI-6400 system at the time of measurement.

No summer photosynthesis data was collected at any locations in 2011 because of an instrument exposure to salt-water that required extensive repairs. Data were not collected at the control location in August and September 2010 since we assume that photosynthesis and its variability are similar to those in July, as the daily average air temperature for the three months were similar (28.3 °C in July, 28.9 °C in August and 26.7 °C in September). In order to assess the recovery of photosynthesis at the impacted locations (medium, heavy), we assume that their close proximity to the control location provided similar environmental conditions.

2.3. Developing the spatio-temporal hierarchical Bayesian model

In order to model photosynthesis, we started with a saturation function to simulate the response of photosynthesis to PAR intensity, the photosynthesis–irradiance (*P–I*) curve. We made the model stochastic to reflect the fact that there

is inherent natural variability in the saturation function that describes photosynthesis versus PAR. Furthermore, we acknowledged that the variability among individual plants, micro-site variability and temporal variability can all affect photosynthesis in unpredictable ways.

The recognition of these multiple sources of natural spatial and temporal variability guided the development of the process and parameter levels in our HB model (figure 2 and table 1). The goal of the model was to estimate photosynthesis rates as a function of (1) the covariate at the leaf scale: PAR, (2) the covariates at the individual scale: air temperature and stress/health level, (3) the covariate at the micro-site scale: the level of crude oil contamination, and (4) the covariate at the temporal scale: the number of days after the beginning of crude oil impact (8 July 2010).

To represent these functions, let *i* represent month, *j* represent location, *k* represent an individual, *l* represent PAR intensity (unit: μmol photon m^{-2} s^{-1}), P_{ijkl} represent the photosynthesis rate (μmol C m^{-2} s^{-1}) at PAR intensity *l* for individual *k* at location *j* at month *i* (as we have photosynthesis measurements for each month). Let $P_{ijkl}.\mu$ represent the mean of P_{ijkl}, σ_L^2 represent the variance of the photosynthesis rates among the 5 different PAR values (~400, 800, 1200, 1600, 2000 μmol photon m^{-2} s^{-1}) at the leaf scale. *N* represent a normal distribution, ~ represent 'is distributed as', so P_{ijkl} is modeled using equation (1):

$$P_{ijkl} \sim N(P_{ijkl}.\mu, \sigma_L^2). \tag{1}$$

(Note: photosynthesis can be negative when the leaves were covered by crude oil.)

Table 1. Summary of the parameters and state variables in the model (note the symbol does not include the subscripts (note: subscripts: i = month; j = micro-site (location); k = individual; l = PAR level) in the equations).

Scales	Symbols representing the parameters or state variables	Meaning
Global scale	θ_0	Global intercept
Micro-site scale (f_{MS})	Time	Days after the initial impact (8 July 2010) (unit: days)
	Loc_m	Dummy variable to represent whether the location is medium impacted location (1) or not (0)
	Loc_h	Dummy variable to represent whether the location is heavily impacted location (1) or not (0)
	$\alpha_0, \alpha_0.\mu$	Intercept at the micro-site scale, mean of the intercept
	θ_1	Coefficient for Time
	θ_2	Coefficient for Loc_m
	θ_3	Coefficient for Loc_h
	$\sigma_{MS}^2 (\tau_{MS} = 1/\sigma_{MS}^2)$	Variance (precision = inverse of variance) at the micro-scale process
Individual scale (f_K)	T	Air temperature (unit: °C)
	S	Stress/health status represented by F_v/F_m[a]
	$\beta_0, \beta_0.\mu$	Intercept at the individual scale, mean of the intercept
	α_1	Coefficient for T
	α_2	Coefficient for S
	$\sigma_K^2 (\tau_K)$	Variance (precision) at the individual-scale process
Leaf scale (f_L)	PAR	Photosynthetically active radiation (unit: μmol photon m^{-2} s^{-1})
	P	Photosynthesis rate (unit: μmol C m^{-2} s^{-1})
	$P.\mu$	Mean of the photosynthesis rate (unit: μmol C m^{-2} s^{-1})
	ω	Half-saturation irradiance (assuming PAR0 = 0) (unit: μmol photon m^{-2} s^{-1})
	z	Transformed variable: $z = $ PAR$/(\omega + $ PAR$)$
	PAR0	Compensation irradiance (unit: μmol photon m^{-2} s^{-1})
	Pmax	Maximum photosynthesis rate
	β_1	Coefficient for z
	$\sigma_L^2 (\tau_L)$	Variance (precision) at the leaf scale process

[a] $F_v = F_m - F_o$, F_o is the minimum fluorescence in dark adapted leaves, and F_m is the maximum fluorescence in dark adapted leaves. For healthy plants, F_v/F_m is between 0.75 and 0.85. The lower the F_v/F_m, the more stressed the leaf (LI-COR Inc. 2003).

We applied a Michaelis–Menten equation to model $P_{ijkl}.\mu$ as a function (f_L) of available PAR at the leaf scale (equation (2)):

$$P_{ijkl}.\mu = f_L(\text{Pmax}_{ijk}, \text{PAR0}_{ijk}, \omega)$$
$$= \text{Pmax}_{ijk} \frac{\text{PAR}_{ijkl} - \text{PAR0}_{ijk}}{\omega + \text{PAR}_{ijkl}} \quad (2)$$

where Pmax_{ijk} (μmol C m^{-2} s^{-1}), PAR0_{ijk} (μmol photon m^{-2} s^{-1}), and ω (μmol photon m^{-2} s^{-1}) are the three parameters that need estimation. Pmax_{ijk} represents the maximum net photosynthesis rate, PAR0_{ijk} represents the PAR intensity where net photosynthesis becomes positive (called the compensation irradiance), and ω represents the PAR intensity when the photosynthesis is half of the Pmax_{ijk} (assuming PAR0_{ijk} is 0; called half-saturation irradiance).

We reparameterized the nonlinear Michaelis–Menten equation to make it linear so we could derive the posteriors more efficiently (Clark *et al* 2003, Clark 2007). To do this, the new variable that replaces PAR_{ijkl} is $z_{ijkl} = \frac{\text{PAR}_{ijkl}}{\omega + \text{PAR}_{ijkl}}$, so that $P_{ijkl}.\mu$ can now be modeled as a linear function of z_{ijkl} (equation (3)):

$$P_{ijkl}.\mu = f_L(\beta_{0ijk}, \beta_1) = \beta_{0ijk} + \beta_1 z_{ijkl}. \quad (3)$$

The new parameters β_{0ijk} and β_1 represent the intercept modeled from the individual scale and the coefficient for the transformed variable z_{ijkl}, respectively, and they are related to the original parameters through equations (4) and (5):

$$\text{Pmax}_{ijk} = \beta_{0ijk} + \beta_1 \quad (4)$$

$$\text{PAR0}_{ijk} = -\beta_{0ijk}\omega(\beta_{0ijk} + \beta_1)^{-1}. \quad (5)$$

Therefore, P (photosynthesis rates) for n_1 PAR intensities per individual, n_2 individuals per location at n_3 locations over n_4 months is modeled as in equation (6):

$$p(P|\beta_0, \beta_1, \sigma_L^2) \propto \prod_{i=1}^{n_4} \prod_{j=1}^{n_3} \prod_{k=1}^{n_2} \prod_{l=1}^{n_1}$$
$$N(P_{ijkl}|f_L(\beta_{0ijk}, \beta_1), \sigma_L^2) \quad (6)$$

where $\propto$ denotes 'is proportional to'.

At the individual scale,

$$\beta_{0ijk} \sim N(\beta_{0ijk}.\mu, \sigma_K^2) \quad (7)$$

where $\beta_{0ijk}.\mu$ is the mean of β_{0ijk}, and σ_K^2 is the variance at the individual scale. In equation (7) $\beta_{0ijk}.\mu$ is a function of air temperature (T_{ijk}) and stress level (S_{ijk}) (measured as F_v/F_m) for individual k at location j at month i, as defined by

equation (8):

$$\beta_{0ijk}.\mu = f_K(\alpha_{0ij}, \alpha_1, \alpha_2) = \alpha_{0ij} + \alpha_1 T_{ijk} + \alpha_2 S_{ijk} \tag{8}$$

where α_{0ij} is the intercept modeled from the micro-site scale (among the 3 locations), α_1 and α_2 are the coefficients for T_{ijk} and S_{ijk} respectively,

Therefore, β_0 is modeled as equation (9):

$$p(\beta_0 \mid \alpha_0, \alpha_1, \alpha_{2,}\sigma_K^2)$$
$$\propto \prod_{i=1}^{n_4}\prod_{j=1}^{n_3}\prod_{k=1}^{n_2} N(\beta_{0ijk} \mid f_K(\alpha_{0ij}, \alpha_1, \alpha_2), \sigma_K^2). \tag{9}$$

At the micro-site scale, α_{0ij} is modeled using equation (10):

$$\alpha_{0ij} \sim N(\alpha_{0ij}.\mu, \sigma_{MS}^2) \tag{10}$$

where $\alpha_{0ij}.\mu$ is the mean of α_{0ij}, σ_{MS}^2 is the variance at the micro-site scale. In equation (10), $\alpha_{0ij}.\mu$ is modeled as a function of the days after the initial oil impact (Time$_i$), and two dummy variables representing the locations that have medium (Loc$_m$) and heavy impact (Loc$_h$) from crude oil contamination as defined in equation (11):

$$\alpha_{0ij}.\mu = f_{MS}(\theta_0, \theta_1, \theta_2, \theta_3)$$
$$= \theta_0 + \theta_1[\text{Loc}] \times \text{Time}_i + \theta_2$$
$$\times \text{Loc}_m + \theta_3 \times \text{Loc}_h \tag{11}$$

where θ_0 is the global intercept, θ_1 is a vector of coefficients for the days after the initial impact (Time) at each location (Loc), θ_2 is the coefficient for the dummy variable of medium location Loc$_m$, and θ_3 is the coefficient for the dummy variable of heavy location Loc$_h$. The dummy variables Loc$_m$ and Loc$_h$ will only take the values of 0 or 1. If Loc$_m$ is 1, then $\alpha_{0ij}.\mu$ represents the mean of α_{0ij} for the medium impacted location; if Loc$_h$ is 1, then $\alpha_{0ij}.\mu$ represents the mean of α_{0ij} for the heavily impacted location; if both Loc$_m$ and Loc$_h$ are 0s, then $\alpha_{0ij}.\mu$ represents the mean of α_{0ij} for the control location; at no time can Loc$_m$ and Loc$_m$ be 1 at the same time.

Therefore, α_0 is modeled as equation (12):

$$p(\alpha_0 \mid \theta_0, \theta_1, \theta_2, \theta_3, \sigma_{MS}^2)$$
$$\propto \prod_{i=1}^{n_4}\prod_{j=1}^{n_3} N(\alpha_{0ij} \mid f_{MS}(\theta_0, \theta_1, \theta_2, \theta_3), \sigma_{MS}^2). \tag{12}$$

To complete the Bayesian model, we require prior distributions for unknown parameters (αs, βs, θs and σs) described above. We used priors that were conjugate with the likelihood for computation efficiency (Calder *et al* 2003), meaning that prior and posterior distributions had the same form. For instance, the variance parameters $\sigma_L^2, \sigma_K^2, \sigma_{MS}^2$ had inverse gamma (IG) priors, which is conjugate for the normal likelihood distribution. For the other parameters, we used normal distributions as priors. The priors are 'non-informative', meaning that the prior distributions were rather flat and only weakly influenced the parameter estimates since we knew little about the unknown parameters (Hartigan 1998, Clark and Bjornstad 2004).

By combining the parameter, process, and data models as defined above in equations (1)–(12), we derived the joint posterior (equation (13)):

$$p(\beta_0, \beta_1, \alpha_0, \alpha_1, \alpha_2, \theta_0, \theta_1, \theta_2, \theta_3, \sigma_L^2, \sigma_K^2, \sigma_{MS}^2 \mid P,$$
$$\quad \text{PAR}, T, S, \text{Time}, \text{Loc}_m, \text{Loc}_h, \text{priors})$$
$$\propto p(P \mid \beta_0, \beta_1, \sigma_L^2)$$
$$\times p(\beta_0 \mid \alpha_0, \alpha_1, \alpha_2, \sigma_K^2) \times p(\alpha_0 \mid \theta_0, \theta_1, \theta_2, \theta_3, \sigma_{MS}^2)$$
$$\times p(\theta_0) \times p(\theta_1) \times p(\theta_2) \times p(\theta_3)$$
$$\times p(\alpha_1) \times p(\alpha_2) \times p(\beta_1)$$
$$\times p(\sigma_L^2) \times p(\sigma_K^2) \times p(\sigma_{MS}^2) \tag{13}$$

From the model just described, we could infer (1) the impact of the PAR intensity (β_1, ω), air temperature (α_1) and stress level (α_2) on photosynthesis rates, (2) the temporal trend of photosynthesis at each location (θ_1), (3) how photosynthesis at the impacted locations compared to the control location over time (α_0), and (4) which spatial scale contributed most to variability in photosynthesis rates (τ). In particular, we are interested in using the model to infer when the photosynthesis at the impacted locations started to recover to similar rates as the control location, and which spatial scale contributes the most to variability in the photosynthesis simulations.

2.4. Implementing the hierarchical Bayesian model

We implemented the model described in equation (13) using Markov Chain Monte Carlo (MCMC) simulations (Gelfand and Smith 1990) in the software OpenBugs 3.2.1 (Rev. 781). We evaluated convergence of the parameters (αs, βs, θs and σs) by simulating three MCMC chains from three different sets of initial values (figure S1 available at stacks. iop.org/ERL/7/045302/mmedia). The chains converged based on Gelman and Rubin's convergence statistics (Brooks and Gelman 1998) and convergence required 90 000 iterations of MCMC. These pre-convergence 'burn-in' iterations were discarded and an additional 90 000 iterations were saved for the subsequent analysis. The upper 95% confidence limit of the convergence statistics for the parameters, latent variables and variances based on the post-burn-in iterations are all less than 1.2, indicating that the chains converged to the stable posterior distribution (Clark 2007).

We used an index of agreement (IoA) to assess the match between simulated medians of photosynthesis and the measured photosynthesis (equation (14): Willmott *et al* 1985, 2012):

$$\text{IoA} = 1 - \frac{\sum_{i=1}^{n} |\text{Pr}_i - O_i|}{\sum_{i=1}^{n}(|\text{Pr}_i - \bar{O}| + |O_i - \bar{O}|)} \tag{14}$$

where Pr_i is the model predictions, O_i is the observed (or measured) data, $\bar{O}$ is the average of observed (measured) data, and n is the number of data points. IoA measures the agreement between predictions and observations on a one-by-one basis. This dimensionless index ranges from 0.0 (indicating no agreement) to 1.0 (perfect agreement). It approaches 1.0 slowly as Pr approaches O, and therefore, provides a reliable tool to assess the model's performance.

Figure 3. Plots of medians with 95% confidence intervals for the measured photosynthesis rate (μmol C m^{-2} s^{-1} − y axis) at different photosynthetic active radiation (PAR) (*x*-axis) at the locations of (A) control, (B) medium impact, and (C) heavy impact in each month from July 2010 to November 2011. At the *x*-axis, 1 = the PAR around 400 μmol C m^{-2} s^{-1}, 2 = the PAR around 800 μmol C m^{-2} s^{-1}, 3 = the PAR around 1200 μmol C m^{-2} s^{-1}, 4 = the PAR around 1600 μmol C m^{-2} s^{-1}, and 5 = the PAR around 2000 μmol C m^{-2} s^{-1}. Note: (1) we do not have measurements of June to August 2011 due to the equipment breakdown; (2) we do not have measurements of photosynthesis in August and September 2010 at the control location and we assume they were similar to the photosynthesis at the same location in July 2010; (3) we do not have measurements of photosynthesis in October 2010 and February 2010 at the medium location; and (4) we have only one individual's measurements in October 2010 at the heavy location after removal of the questionable data.

2.5. Modifying the hierarchical Bayesian model

We also explored possible improvements to the model by modifying equation (11) to include Julian days as a covariate to represent seasonality (equation (15)):

$$\alpha_{0ij}.\mu = f_{\text{MS}}(\theta_0, \theta_1, \theta_2, \theta_3, \theta_4, \theta_4) = \theta_0 + \theta_1[\text{Loc}]$$
$$\times \text{Time}_i + \theta_2 \times \text{Loc}_m + \theta_3 \times \text{Loc}_h + \theta_4$$
$$\times \text{JulianDay} - \theta_5 \times \text{JulianDay}^2. \qquad (15)$$

For the effect of Julian day, we wanted a model that would have a single peak value to represent the highest photosynthesis rates in the late spring or summer (between Julian days 120 and 240), so θ_5 should be positive in equation (15).

We also considered other modifications to the initial model (equation (13)) to improve the photosynthesis simulation: (a) possible nonlinear effect of temperature (equation (16)), and (b) possible interaction between air temperature and stress status of the plants (equation (17)) at the individual scale, so we modified equation (8) to:

$$\beta_{0ijk}.\mu = f_K(\alpha_{0ij}, \alpha_1, \alpha_2)$$
$$= \alpha_{0ij} + \alpha_1 T_{ijk} + \alpha_2 S_{ijk} - \alpha_3 T_{ijk}^2 \qquad (16)$$

and

$$\beta_{0ijk}.\mu = f_K(\alpha_{0ij}, \alpha_1, \alpha_2)$$
$$= \alpha_{0ij} + \alpha_1 T_{ijk} + \alpha_2 S_{ijk} + \alpha_4 T_{ijk} S_{ijk}. \qquad (17)$$

In particular, we assessed the significance of the coefficients for the added covariates and how the added covariates affect the coefficient estimates for the other covariates.

3. Results

3.1. Measured photosynthesis rates

Not all field measurements obtained were used in the model; 17.7% of the data were removed from our data analysis and model development. Some examples of data that were exclude are: too small a leaf area in the leaf chamber, negative values which could not be explained by health status of the leaves (as indicated by the field notes and F_v/F_m measurements), or the response of photosynthetic rates being much smaller under high PAR levels compared to low PAR levels but do not represent photoinhibition.

At the control location, measured photosynthesis rates were high (41.29 ± 13.17 (standard deviation) μmol C m^{-2} s^{-1}) compared to medium (26.27 ± 10.71 μmol C m^{-2} s^{-1}) and heavy impact locations (−1.53 ± 0.783 μmol C m^{-2} s^{-1}) in July 2010 (figure 3). Late fall and winter (Nov 2010–Feb 2011) photosynthesis rates were low (15.84 ± 6.33 μmol C m^{-2} s^{-1}), and began to increase in March 2011 at the onset of the growing season of *S. alterniflora* (figure 3).

Photosynthesis at the medium oiled location was lower than at the control location in July 2010 and the mean rate

Table 2. Summary of the quantiles and the means of selected parameters simulated from the HB model.

Parameters		2.5% quantile	Median	Mean	97.5% quantile
θ_0 (global intercept)		−42.359	−24.761	−25.045	−9.275
θ_1 (temporal trend)	Control	−0.0596	−0.0407	−0.0407	−0.0219
	Heavy	−0.0102	0.008 41	0.008 42	0.0272
	Medium	−0.0276	−0.008 25	−0.008 27	0.0110
θ_2 (medium location)		−19.024	−11.180	−11.170	−3.266
θ_3 (heavy location)		−28.681	−21.089	−21.106	−13.617
α_1 (air temperature)		0.0331	0.281	0.280	0.515
α_2 (leaf stress, F_v/F_m)		3.992	11.291	11.255	18.508
β_1 (transformed PAR)		42.058	52.803	53.161	66.543
ω (μmol photon m^{-2} s^{-1}) (half-saturation PAR intensity)		138.667	201.837	209.258	315.020
τ_{MS} (precision at micro-site scale)		0.0250	0.0451	0.0471	0.0806
τ_K (precision at individual scale)		0.0233	0.0285	0.0286	0.0346
τ_L (precision at the leaf scale)		0.0472	0.0513	0.0514	0.0557

decreased in September 2010. As for the control location, mean photosynthesis rates declined during the winter before increasing during the spring 2011 growing season (figure 3). Measured photosynthesis was negative (i.e., respiration only) at the heavily oiled location in July 2010 and photosynthesis rates at this location started to increase in August and September 2010. At that time, new leaves were observed to grow back from the roots unaffected by oil toxicity and replace dead leaves coated by crude oil. During the winter months of 2010–2011, the contrast between the photosynthesis rate at the control location and the two impacted locations was not as obvious as just after the oil impact in the summer of 2010 (figure 3). *S. alterniflora* undergoes senescence of above-ground tissues in winter as it is not an evergreen (Edwards and Mills 2005). Photosynthesis increased through spring 2011 at all three locations during the period of active new growth, no summer data were available due to instrument malfunction, and photosynthesis decreased again starting in October at the control location, and September at the medium and heavily impacted locations.

3.2. Simulated photosynthesis

3.2.1. Model comparison.
The simulation results showed that the coefficients for the quadratic term of Julian day θ_5 in equation (15) was significant larger than 0 (95% credible interval, 2.5% quantile to 97.5% quantile: 1.7555×10^{-6}–5.5201×10^{-4}), meaning that seasonality represented by Julian day significantly affected simulated photosynthesis rates. Meanwhile the coefficient for air temperature α_1 was not significantly different from 0 (95% credible interval: −0.4977–0.1150), meaning that air temperature did not significantly affect simulated photosynthesis once the seasonality has been accounted for by Julian day. When the original equation (11) was applied, the 95% credible interval of the coefficient for air temperature α_1 was positive (table 2) meaning that air temperature significantly affected simulated photosynthesis. These indicated that air

temperature accounted for seasonality in the original model while Julian day accounted seasonality in the revised model. However, the penalty due to the inclusion of more parameters related to Julian day made the revised model have a larger Bayesian deviance information criterion (DIC = 8452) compared to the original model (DIC = 8430), suggesting that Julian day was not a better explanatory covariate for seasonal photosynthesis response than air temperature alone. The posteriors of the coefficient for the quadratic term of air temperature (α_3) in equation (16) (95% credible interval: −0.04351–0.01788), and the coefficient for the interaction of air temperature and stress level (α_4) in equation (17) (95% credible interval: −1.2685–0.9009), ranged from negative to positive. This indicated there were no significant nonlinear effects of air temperature, or the interaction of air temperature with health/stress level. Therefore, we believe the air temperature in the original model effectively accounted for temperature variability in the simulated photosynthesis rates over the different seasons. Since no modification improved the original model, the following simulation results were based on the original model (equation (13)).

3.2.2. Model performance.
The density distributions of the medians of simulated photosynthesis rates from the HB model matched those of the measured photosynthesis well across the three locations, especially at the heavy impact location (figure 4). The good match between the simulated medians and the measured data was also shown in the IoA, which was 0.835 at the control and medium oiled locations, and 0.842 at the heavily oiled location. The posteriors of the simulated photosynthesis captured most of the variability of measured photosynthesis (figure 5). These all suggested the HB model performed well in simulating the observed photosynthesis.

3.2.3. Simulation posteriors.
The photosynthesis rate at the control location showed a decreasing trend from July 2010 to November 2011 as the 95% credible interval of the parameter (θ_1[control]) was negative (table 2 and figure S2
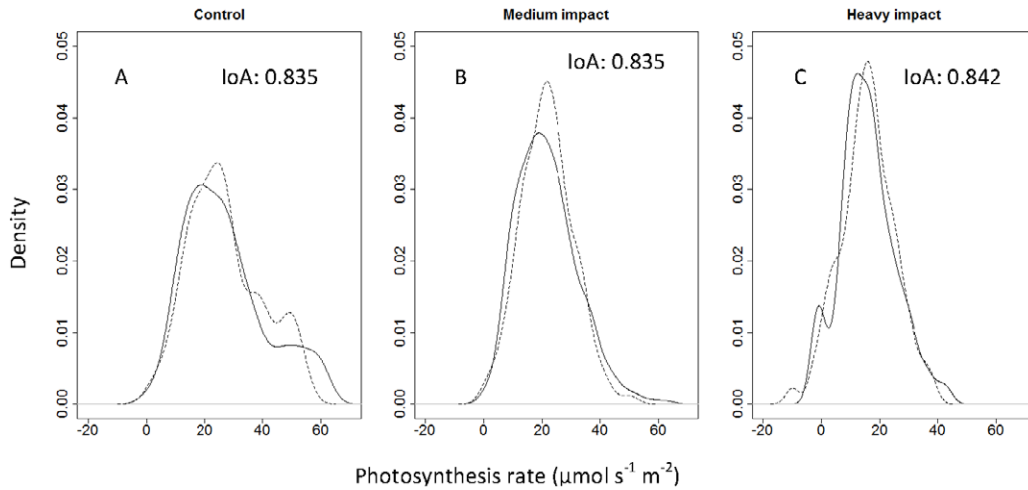
8

Figure 4. Density distributions of measured photosynthesis rates (solid lines) and medians of simulated photosynthesis posteriors (dashed lines) at the locations of (A) control, (B) medium impact and (C) heavy impact. (IoA: index of agreement.)
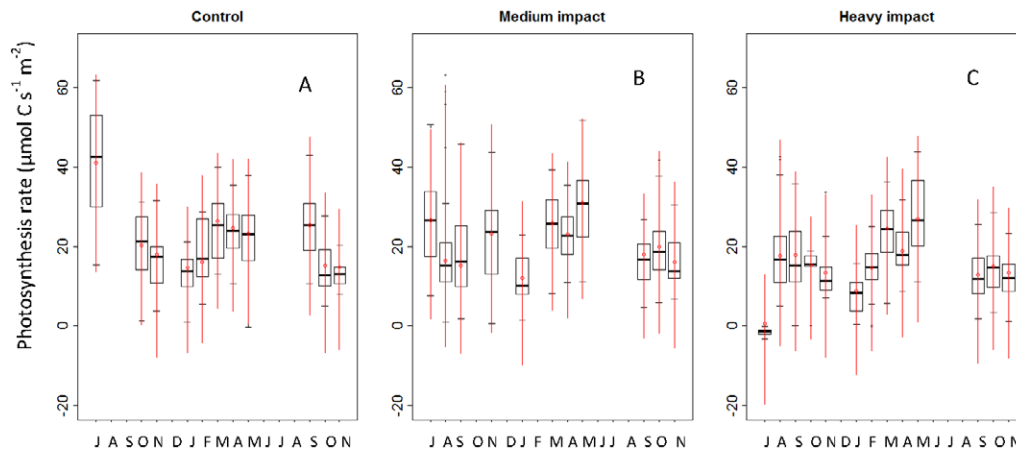

Figure 5. Simulated photosynthesis rates with 95% credible intervals (red points: medians; red lines: 95% credible intervals) each month (starting with July 'J') at the locations of (A) control, (B) medium impact and (C) heavy impact. Boxplots contrast these values with the measured photosynthesis rates (black) starting with July 2010.

(available at stacks.iop.org/ERL/7/045302/mmedia); note, missing measurements August and September 2010 and June–August 2011). At the two impacted locations, there was not an apparent trend of the simulated photosynthesis rates over the same time period, though the medians of the change rates were positive at the heavy and negative at the medium locations. The 95% credible intervals for θ_1[control] and θ_1[heavy] did not overlap, showing a significantly different temporal trend (table 2) at the control and heavy locations. The overlapping of the 95% credible intervals between the medium and control locations was small, and there did not show a significant difference in temporal trend between the medium and control locations or the medium and heavy locations.

PAR and air temperature positively affected photosynthesis since the 95% credible intervals of β_1 (transformed PAR) and α_1 (air temperature) were positive (table 2, figures S3 and S4 available at stacks.iop.org/ERL/7/045302/mmedia). The positive 95% credible interval of α_2 (leaf stress) indicated that the higher the F_v/F_m (less stress), the higher the

photosynthesis (table 2 and figure S3 available at stacks.iop.org/ERL/7/045302/mmedia). The 95% credible interval for omega was 138.667–315.020 μmol photon m^{-2} s^{-1} (table 2 and figure S4 available at stacks.iop.org/ERL/7/045302/mmedia) suggesting that this species can reach half of the maximum photosynthesis rate at that range of irradiance.

The medians for photosynthesis rate at the leaf scale (P) and the intercept at the individual scale (β_0) were of a similar magnitude (20.70 and 22.62), and the median of the intercept from the micro-site scale (α_0) was about twice as large as those at finer scales (39.38). In terms of variability, the individual scale (τ_K) showed lower precision (inverse of variance, see table 1) and precision/median ratio (normalized precision) compared to the leaf scale (τ_L), which indicates that individual variability contributes more to the simulated photosynthesis rates than does leaf scale variance (table 2 and figure S5 available at stacks.iop.org/ERL/7/045302/mmedia). At the micro-scale (τ_{MS}), which includes both spatial and temporal variability, the precision and the precision/median ratio ranged from low to high (table 2). The 97.5% quantile
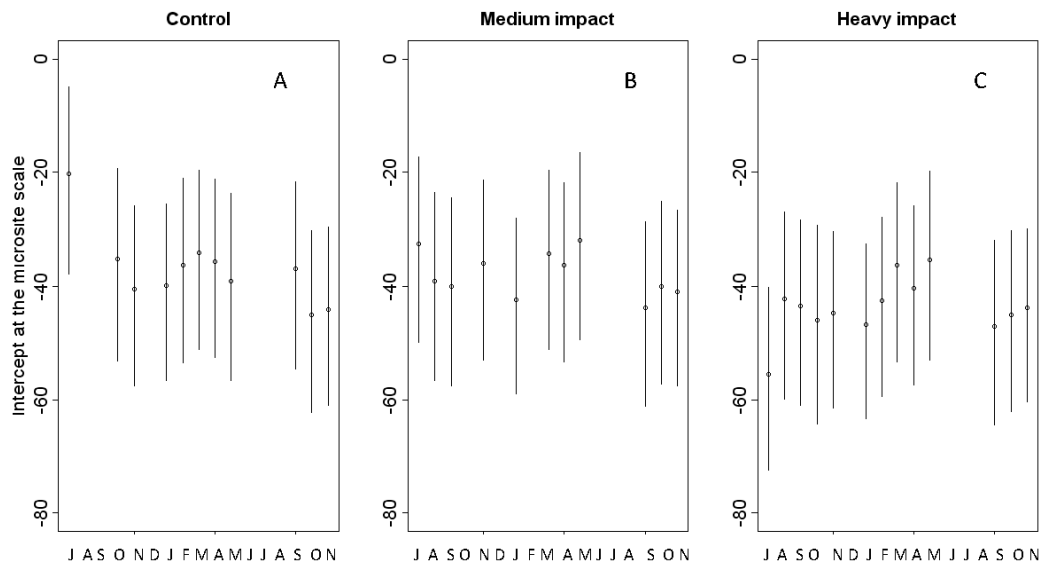
Figure 6. The intercept of the micro-site scale (α_0) which indicates temporal trend of photosynthesis (starting with July 'J') at the locations of (A) control, (B) medium impact and (C) heavy impact for each month starting with July 2010. The dots represent the medians of α_0 and the black lines represent the 95% credible intervals.

of precision/median at the micro-site scale (τ_{MS}) is lower than 2.5% quantile of precision/median at the leaf scale (τ_L) (table 2), showing the normalized precision at the leaf scale is significantly higher than that at the micro-site scale. These indicate the uncertainties in modeling photosynthesis rates mainly came from the variability at the individual and micro-site scales, less from the leaf scale.

3.2.4. The monthly trend of the difference between the impacted locations and the control location. The monthly trend of photosynthesis modeled by the HB at each location can be summarized using the intercept at the micro-scale, α_0 (figure 6 and equations (10)–(12)). The value of α_0 was different from the actual photosynthesis as it was standardized for the covariates of PAR intensity, air temperature and F_v/F_m. At the beginning of the study (after the acute oil impact in July 2010), the 95% credible intervals of α_0 for the control (-37.893, -4.839) and heavy impact locations (-72.532, -40.283) did not overlap. This indicates that there existed significant differences in photosynthesis between these locations. The medians at the heavy (-55.415) and medium (-32.540) locations were smaller than at the control location (-20.265) in July 2010, indicating that median photosynthesis was lower at the two oil impacted locations than the adjacent control location. Over the course of the study, the amount of overlap of the 95% credible intervals among the three locations increased through time, and the medians of the photosynthesis rates at the two impacted locations approached the control location suggesting recovery by the plants. By the end of the study in November 2011, the simulated α_0 had medians of -44.143, -43.826 and -40.924 at the control, medium and heavy locations, respectively, with 95% credible intervals (-60.915, -39.577), (-60.358, -29.851) and (-57.507, -26.677) (figure 6). This indicated photosynthesis at the impacted locations had recovered to the status of the control location after 16 months.

4. Discussion

Studies of the impact of oil spills on salt marsh plants have been focused on Louisiana due to more frequent oil spill events and large marsh areas there (Pezeshki and DeLaune 1993, Pezeshki *et al* 2000, Hester and Mendelssohn 2000, Ko and Day 2004, Mishra *et al* 2012, Mendelssohn *et al* 2012). During the DWH oil spill, marsh shorelines and not the marsh interior were exposed to the weathered oil (Mendelssohn *et al* 2012). Limited quantitative data are yet available on the impact of DWH oil spill on salt marsh vegetation. Mishra *et al* (2012) assessed the ecological impact on the salt marshes along the southeastern Louisiana coast using photosynthetic capacity and physiological status through satellite and ground truth data, and found extensive reduction in photosynthetic activity during the peak of the growing season in 2010. Lin and Mendelssohn (2012) documented variable impacts depending on oiling intensity in the Bay Jimmy, northern Barataria Bay, Louisiana. As of the fall of 2011, many of the most heavily oiled shorelines had minimal to no recovery (Mendelssohn *et al* 2012). In Mississippi, some salt marshes experienced crude oil impact, such as in Davis Bayou, Grand Bay, Garden Pond at Horn Island and in Waveland, but the impact and recovery have not attracted enough attention or been documented well. This paper enhances our understanding of the impacts of the DWH oil spill on photosynthesis of the dominant marsh plant, *S. alterniflora*, from Mississippi.

To improve our understanding of oil's impact on coastal salt marsh plants, we used an HB modeling approach because it can assimilate data and account for variability at multiple spatial and temporal scales in a coherent framework (e.g., McMahon and Diez 2007, Clark *et al* 2011, Wilson *et al* 2011). An HB model has been applied to monitor long-term harbor seal abundance changes in Prince William Sound, Alaska impacted by the 1989 Exxon Valdez oil spill (ver Hoef
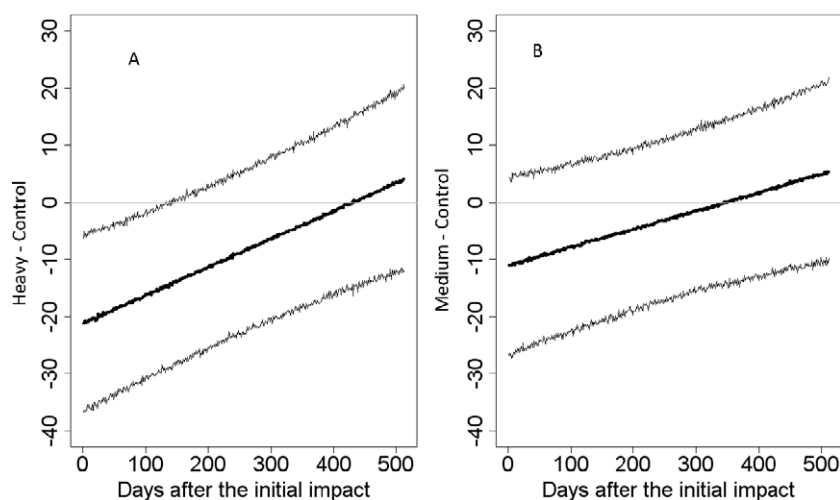
Figure 7. Photosynthesis difference between the impacted locations ((A) heavy location; (B) medium location) and the control location over time. The thin lines represent 2.5% and 97.5% quantiles, and the think lines represent medians of the difference. The vertical space between 2.5% and 97.5% quantiles shows the 95% predictive intervals. The gray line represents the horizontal line at 0 and vertical line at day 140 when photosynthesis at the heavy oiled location stated to recover to the level at the control location.

and Frost 2003). However, HB models have not been applied to assess the impact of oil spill's on coastal salt marsh.

Other types of saturation curves and mechanistic models are available to model photosynthesis (e.g., Jassby and Platt 1976, Chalker 1981, Thornley and Johnson 1990, Farquhar *et al* 1980, Farquhar and von Gaemmerer 1982, Farquhar *et al* 2001, Marino *et al* 2010). The application of the Michaelis–Menten function adequately accounted for the relation between photosynthesis and PAR intensity, and facilitated the inference on the temporal trend of photosynthesis and its contrast between the impacted and the control locations, as the leaf scale contributed the least to the variability in the photosynthesis simulations.

During the winter months in 2010, the contrast between the control and the two impacted locations in the field data was not as obvious as during the growing season earlier in 2010. This could be explained either by complete recovery of photosynthesis from oil impacts, or it could be due to seasonally lower air temperature being a limiting factor keeping photosynthesis uniformly low. Due to the uncertainty surrounding the interpretation of the field data, we relied on the HB model to derive a temporal pattern of simulated photosynthesis at the three study locations standardized for seasonality, PAR intensity, and individual variability. The linear coefficient θ_1 in the model may oversimplify the temporal trend at each location. However, it captured the general trend of photosynthesis change, although smoothing over small fluctuations (Ver Hoef and Frost 2003).

In particular, we used the HB model to predict the time course of photosynthetic recovery at the impacted locations to values similar to the control location. In order to derive when photosynthesis had recovered to the status of the control location, a finer temporal resolution than month would be required. We applied the posteriors of $\theta_0 - \theta_3$ and τ_{MS} in equations (10)–(12) from our HB model to generate the predictive α_0 at each day after the initial impact at each location. Then, the difference of α_0 between heavy and

control locations and between medium and control locations were calculated. The 2.5% and 97.5% quantiles and medians of the differences of each day were derived (figure 7). The generally increasing trend over time in the differences between the impacted and control locations was largely due to the decreasing trend at the control location. If the 95% credible intervals of the difference included 0, then the photosynthesis rates between the impacted and the control locations did not show a significant difference. Based on this, we could derive the photosynthesis rates at the heavy location recovered to the status of the control location about 140 days (4.7 months) after the initial impact, which was in early December 2010 (figure 7(A)). On the other hand, the oil impact was never severe enough to make the photosynthesis rates at the medium location significant lower than that at the control location (figure 7(B)).

There are two possible reasons photosynthesis recovered so quickly. First, the small concentration and very patchy distribution of crude oil associated with salt marsh plants (Biber *et al* in review) showed the roots were possibly free of contamination, which led to quick regrowth of leaves at the heavily oiled location. At the beginning of the crude oil impact (July 2010), the concentration of oil range organics (C19–C36) ranged from 37 000 to 48 900 mg kg^{-1} (ppm) on the plants and 32.4–44.2 ppm in the sediment at the heavy impacted location. The detailed chemical analysis of saturated hydrocarbons on the oil collected confirmed that it most likely came from the BP DWH spill as the GC-FID chromatograms showed a similar distribution pattern of resolved peaks and unresolved complex mixture compared to the MC252 reference oil source from BP (Liu *et al* 2012). The concentration dropped to 686–1070 ppm on the plants and <50 ppm in the sediment at the impacted location by October 2010. Second, quick natural degradation and possible physical removal by waves and tides at the study area reduced the amount of crude oil that washed ashore in the salt marsh. In particular, areas exposed to the predominant

southeasterly winds, common during the summer in our study area, experienced substantial tidal 'cleaning' with oil being removed during high tides and periods of strong wave action corresponding to tropical storms in the GOM. Warm temperatures, often exceeding 35 °C during the day are also common in the region from June through September, promoting rapid volatilization of lighter carbon fractions which correlates to reduced toxicity (Irwin *et al* 1997).

5. Synthesis

Our study demonstrated a relatively new approach to assess ecological recovery—the HB modeling approach. It shows a promising tool to assess wetland's resilience to disturbance by accounting for uncertainties from different sources at different spatial and temporal scales in a coherent framework. The application of our HB model facilitated a better understanding of oil impacts to *S. alterniflora* and generated inference we could not have obtained from the empirical data alone. For example, (1) air temperature and PAR positively influenced photosynthesis, whereas the leaf stress level negatively affected photosynthesis, (2) the overall temporal changes in photosynthesis rates with standardized covariates over 17 months had a negative trend at the control location, and ranging from negative to positive trend at the impacted locations, (3) the photosynthesis rates at the heavily impacted location recovered to the control location about 140 days after the initial impact whereas the impact at the medium location was never large enough to make photosynthesis significantly lower than that at the control location, and (4) the uncertainties in modeling photosynthesis rates mainly came from the variability at the individual and micro-site scales, less from the leaf scale. However, even though photosynthesis had recovered to the status of the control location, we recommend continuous monitoring of photosynthesis rates as (1) longer data will help determine if the decreasing trend at the control location persists and help to explain it, (2) the oil residual buried in the sediment at the fine scale may affect the plant root zone chronically and pose a long-term threat, and (3) accumulating baseline data for assessing the next possible disturbance. Thus, our model approach and results can guide our future sampling efforts in photosynthesis of oil impacted salt marsh plants.

Acknowledgments

References

Alexander S K and Webb J W 1987 Relationship of *Spartina alterniflora* growth to sediment oil content following an oil spill ed American Petroleum Institute *Proc. 1987 Int. Oil Spill Conf. (Washington, DC)* pp 445–9

Baca B J, Lankford T E and Gundlach E R 1987 Recovery of Brittany coastal marshes in the eight years following the Amoco Cadiz incident ed American Petroleum Institute *Proc. 1987 Int. Oil Spill Conf. (Washington, DC)* pp 459–64

Baker J M 1970 The effects of oils on plants *Environ. Pollut.* **1** 27–44

Bergen A, Alderson C, Bergfors R, Aquila C and Matsil M A 2000 Restoration of a *Spartina alterniflora* salt marsh following a fuel oil spill, New York City, NY *Wetl. Ecol. Manag.* **8** 185–95

Biber P D, Wu W, Peterson M S, Liu Z and Pham L, Oil contamination in Mississippi saltmarsh habitats and the impacts to *Spartina alterniflora* photosynthesis *Impacts of Oil Spill Disasters on Marine Habitats and Fisheries in North America* ed B Alford, M S Peterson and C Green (Boca Raton, FL: CRC Press) (in review)

Brooks S P and Gelman A 1998 General methods for monitoring convergence of iterative simulations *J. Comput. Graph. Stat.* **7** 434–55

Burns K A and Teal J M 1979 The west Falmouth oil spill: hydrocarbon in the salt marsh ecosystem *Estuar. Coast. Mar. Sci.* **8** 349–60

Calder C, Lavine M, Muller P and Clark J S 2003 Incorporating multiple sources of stochasticity into dynamic population models *Ecology* **84** 1395–402

Cardoch L, Day J W and Ibanez C 2002 Net primary productivity as an indicator of sustainability in the Ebro and Mississippi deltas *Ecol. Appl.* **12** 1044–55

Chalker B E 1981 Simulating light-saturation curves for photosynthesis and calcification by reef-building corals *Mar. Biol.* **63** 135–41

Clark J S 2005 Why environmental scientists are becoming Bayesians *Ecol. Lett.* **8** 2–14

Clark J S 2007 *Models for Ecological Data* (Princeton, NJ: Princeton University Press) p 617

Clark J S, Bell D M, Hersh M H, Kwit M C, Moran E, Salk C, Stine A, Valle D and Zhu K 2011 Individual-scale variation, species-scale differences: inference needed to understand diversity *Ecol. Lett.* **14** 1273–87

Clark J S and Bjornstad O N 2004 Population time series: process variability, observation errors, missing values, lags, and hidden states *Ecology* **85** 3140–50

Clark J S and LaDeau S L 2006 Synthesizing ecological experiments and observational data with hierarchical Bayes *Hierarchical Models of the Environment* ed J S Clark and A Gelfand (New York: Oxford University Press) pp 41–58

Clark J S, Mohan J, Dietze M and Ibanez I 2003 Coexistence: how to identify trophic trade-offs *Ecology* **84** 17–31

Clark J S *et al* 2001 Ecological forecasts: an emerging imperative *Science* **293** 657–60

Crone T J and Tolstoy M 2010 Magnitude of the 2010 Gulf of Mexico oil leak *Science* **330** 634–4

Dicks B and Hartley J P 1982 The effects of repeated small oil spillages and chronic discharges *Phil. Trans. R. Soc.* B **297** 285–307

Edwards K R and Mills K P 2005 Aboveground and belowground productivity of *Spartina alterniflora* (smooth cordgrass) in natural and created Louisiana salt marshes *Estuaries* **28** 252–65

Eleuterius C K 1998 Oceanography of the Mississippi coastal area *Marine Resources and History of the Mississippi Gulf Coast—Volume II: Mississippi's Coastal Environment* ed L A Klein, M Landry and J E Seward (Biloxi, MS: Mississippi Department of Marine Resources) pp 205–30

Engle V D 2011 Estimating the provision of ecosystem services by Gulf of Mexico coastal wetlands *Wetlands* **31** 179–93

Fabricius K E and De'Ath G 2004 Identifying ecological change and its causes: a case study on coral reefs *Ecol. Appl.* **14** 1448–65

Farquhar G D and von Gaemmerer S 1982 Modeling of photosynthetic responses to environmental conditions *Encyclopedia of Plant Physiology (New Series)* ed O L Lange *et al* (Berlin: Springer) pp 549–87

Farquhar G D, von Caemmerer S and Berry J A 1980 A biochemical model of photosynthetic CO_2 assimilation in leaves of C_3 species *Planta* **149** 78–90

Farquhar G D, von Caemmerer S and Berry J A 2001 Models of photosynthesis *Plant Physiol.* **125** 42–5

Fingas M F 1999 The evaporation of oil spills: development and implementation of new prediction methodology ed American Petroleum Institute *Proc. 1999 Int. Oil Spill Conf. (Washington, DC)* pp 109–14

Gelfand A E and Smith A F M 1990 Sampling-based approaches to calculating marginal densities *J. Am. Stat. Assoc.* **85** 398–409

Gilfillan E S, Maher N P, Krejsa C M, Lanphear M E, Ball C D, Meltzer J B and Page D S 1995 Use of remote sensing to document changes in marsh vegetation following the Amoco Cadiz oil spill (Brittany, 1978) *Mar. Pollut. Bull.* **30** 780–7

Hartigan J A 1998 The maximum likelihood prior *Ann. Stat.* **26** 2083–103

Hester M W and Mendelssohn I A 2000 Long-term recovery of a Louisiana brackish marsh plant community from oil-spill impact: vegetation response and mitigating effects of marsh surface elevation *Mar. Environ. Res.* **49** 233–54

Hunt J M 1996 *Petroleum Geochemistry and Geology* (New York: Freeman)

Irwin R J, van Mouwerik M, Stevens L, Seese M D and Basham W (ed) 1997 Water resources division of National Park Service *Environmental Contaminants Encyclopedia, Crude Oil* (Fort Collins, CO: The National Park Service) p 78

Jassby A D and Platt T 1976 Mathematical formulation of the relationship between photosynthesis and light for phytoplankton *Limnol. Oceanogr.* **21** 540–7

Jordan S J and Peterson M S 2012 Contributions of estuarine habitat to major fisheries *Estuaries: Classification, Ecology, and Human Impacts* ed S J Jordan (Hauppauge, NY: Nova Science Publishers) chapter 5, pp 75–92

Ko J Y and Day J W 2004 A review of ecological impacts of oil and gas development on coastal ecosystems in the Mississippi Delta *Ocean Coast. Manage.* **47** 597–623

Krebs C T and Tanner C E 1981 Restoration of oiled marshes through sediment stripping and *Spartina* propagation ed American Petroleum Institute *Proc. 1981 Int. Oil Spill Conf. (Washington, DC)* pp 375–85

LI-COR Inc. 2003 *Leaf Chamber Fluorometer Using the LI-6400/LI-6400 XT Portable Photosynthesis System* (Lincoln, NE: LI-COR Biosciences) chapter 27, p 27

Lin Q X and Mendelssohn I A 1996 A comparative investigation of the effects of south Louisiana crude oil on the vegetation of fresh, brackish and salt marshes *Mar. Pollut. Bull.* **32** 202–9

Lin Q X and Mendelssohn I A 1998 The combined effects of phytoremediation and biostimulation in enhancing habitat restoration and oil degradation of petroleum contaminated wetlands *Ecol. Eng.* **10** 263–74

Lin Q X and Mendelssohn I A 2012 Impacts and recovery of the Deepwater Horizon oil spill on vegetation structure and function of coastal salt marshes in the Northern Gulf of Mexico *Environ. Sci. Technol.* **46** 3737–43

Liu Z, Liu J, Zhu Q and Wu W 2012 The weathering of oil after the Deepwater Horizon oil spill: insights from the chemical composition of the oil from the sea surface, salt marshes and sediments *Environ. Res. Lett.* **7** 035302

Marino G, Aqil M and Shipley B 2010 The leaf economics spectrum and the prediction of photosynthetic light-response curves *Funct. Ecol.* **24** 263–72

McMahon S M and Diez J M 2007 Scales of association: hierarchical linear models and the measurement of ecological systems *Ecol. Lett.* **10** 437–52

Mendelssohn J A, Hester M W and Hill J M 1993 Assessing the recovery of coastal wetlands from oil spills ed American Petroleum Institute *Proc. 1993 Int. Oil Spill Con. (Washington, DC)* pp 141–5

Mendelssohn I A *et al* 2012 Oil impacts on coastal wetlands: implications for the Mississippi River delta ecosystem after the Deepwater Horizon oil spill *BioScience* **62** 562–74

Michel J, Nixon Z, Dahlin J, Betenbaugh D, White M, Burton D and Turley S 2009 Recovery of interior brackish marshes seven years after the chalk point oil spill *Mar. Pollut. Bull.* **58** 995–1006

Mishra D R, Cho H J, Ghosh S, Fox A, Downs C, Merani P B T, Kirui P, Jackson N and Mishra S 2012 Post-spill state of the marsh: remote estimation of the ecological impact of the Gulf of Mexico oil spill on Louisiana Salt Marshes *Remote Sens. Environ.* **118** 176–85

Naumann J C, Young D R and Anderson J E 2007 Linking leaf chlorophyll fluorescence properties to physiological responses for detection of salt and drought stress in coastal plant species *Physiol. Plantarum* **131** 422–33

Peterson M S and Lowe M R 2009 Implications of cumulative impacts to estuarine and marine habitat quality for fish and invertebrate resources *Rev. Fish. Sci.* **17** 505–23

Pezeshki S R and DeLaune R D 1993 Effect of crude oil on gas exchange functions of *Juncus roemerianus* and *Spartina alterniflora Water Air Soil Pollut.* **68** 461–8

Pezeshki S R, DeLaune R D and Jugsujinda A 2001 The effects of crude oil and the effectiveness of cleaner application following oiling on US Gulf of Mexico coastal marsh plants *Environ. Pollut.* **112** 483–9

Pezeshki S R, Hester M W, Lin Q and Nyman J A 2000 The effects of oil spill and clean-up on dominant US Gulf coast marsh macrophytes: a review *Environ. Pollut.* **108** 129–39

Plata D L, Sharpless C M and Reddy C M 2008 Photochemical degradation of polycyclic aromatic hydrocarbons in oil films *Environ. Sci. Technol.* **42** 2432–8

Reuscher D L Jr 1998 Climatological summary and data for the Mississippi Gulf Coast *Marine Resources and History of the Mississippi Gulf Coast—Volume II: Mississippi's Coastal Environment* ed L A Klein, M Landry and J E Seward (Biloxi, MS: Mississippi Department of Marine Resources) pp 297–304

Roth A M F and Baltz D M 2009 Short-term effects of an oil spill on marsh-edge fishes and decapod crustaceans *Estuar. Coast.* **32** 565–72

Thornley J H M and Johnson I R 1990 *Plant and Crop Modelling—A Mathematical Approach to Plant and Crop Physiology* (Oxford: Clarendon)

Ver Hoef J M and Frost K J 2003 A Bayesian hierarchical model for monitoring harbor seal changes in Prince William Sound, Alaska *Environ. Ecol. Stat.* **10** 201–19

Willmott C J, Ackleson S G, Davis R E, Feddema J J, Klink K M, Legates D R, O'Donnell J and Rowe C M 1985 Statistics for the evaluation of model performance *J. Geophys. Res.* **90** 8995–9005

Willmott C J, Robenson S M and Matsuura K 2012 A refined index of model performance *Int. J. Climatol.* **32** 2088–94

Wilson A M, Silander J A, Gelfand A and Glenn J H 2011 Scaling up: linking field data and remote sensing with a hierarchical model *Int. J. Geogr. Inf. Sci.* **25** 509–21

Wu W, Clark J S and Vose J M 2010 Assimilating multi-source uncertainties of a parsimonious conceptual hydrological model using hierarchical Bayesian modeling *J. Hydrol.* **394** 436–46